

# The effect of a water hammer on cavitating solution of isopropyl alcohol

© S.A. Voropaev<sup>1</sup>, N.V. Dushenko<sup>1</sup>, D.A. Trofimov<sup>1</sup>, A.S. Aronin<sup>2</sup>

<sup>1</sup>V.I. Vernadsky Institute of Geochemistry and Analytical Chemistry, Moscow, Russia

<sup>2</sup>Osipyan Institute of Solid State Physics RAS Russian Academy of Sciences, Chernogolovka, Moscow District, Russia

E-mail: voropaev@geokhi.ru

Received March 11, 2025

Revised April 2, 2025

Accepted April 2, 2025

A study of the effect of the water hammer' magnitude on cavitating aqueous solution of isopropyl alcohol has been conducted. It is shown that with the right amplitude of water hammer, it is possible to form the phase composition of carbon nanoparticles in solution by changing the processes occurring during the collapse of cavitation bubbles. The crystal lattice' parameters of the obtained carbon nanoparticles were measured, and assumptions were made regarding the graphene–diamond composite structure as well as the observed shapes of the nanoparticles.

**Keywords:** carbon, nandiamond, graphene, cavitation, water hammer.

DOI: 10.61011/TPL.2025.07.61422.20311

Graphene, which consists of hexagonally arranged carbon atoms bound by  $sp^2$  hybridization into a single layer [1], has a wide range of promising applications extending from composite materials to quantum dots [2]. However, its availability is limited by the need to overcome the high van der Waals energy ( $5.9 \text{ kJ} \cdot \text{mol}^{-1}$  per carbon atom) with which graphite sheets are bonded to each other. Graphene was first isolated by peeling off mechanically the upper surface of small pieces of pyrolytic graphite [3]. In a different approach, individual sheets of graphene oxide were reduced chemically to graphene after deposition on a silicon substrate [4], which is also a method of limited application.

Exfoliation of graphite oxidized by strong acids either by rapid thermal expansion or by ultrasonic dispersion is one way to obtain functionalized graphene oxide in bulk. The oxidation chemistry is similar to that used for carbon nanotubes [5] at end defect sites. Thus, regardless of the exfoliation mechanics, graphene oxide derived from oxidized graphite has significant oxygen functionality and defects; therefore, one needs to eliminate the associated structural and electronic defects induced by oxidation in order to restore the unique properties of graphene. Ostensibly, these defects may be corrected by „passivation chemistry“ (e.g., in the interaction of graphene oxide with amines [6]). However, it turned out that residual (passivated) defects in the obtained materials do not allow them to replicate completely the electronic properties of graphene.

In the present study, we report on a simple and scalable method for preparation of aqueous solutions of isolated and moderately modified graphene sheet stacks by hydrodynamic (HD) cavitation. This effect was revealed when we examined the feasibility of application of a water hammer in cavitating carbon-containing fluids as a mechanism for synthesis of various nanoforms of carbon [7]. The importance of cavitation as a natural process of diamond nucleation in mantle fluids was predicted in

pioneering studies of Academician E.M. Galimov [8]. To test this hypothesis experimentally, an approach involving the use of HD cavitation in hydrocarbon fluids with a large jump in external pressure ( $\sim 80\text{--}90$  bar) induced by the detonation of a powder charge was developed at the Vernadsky Institute of Geochemistry and Analytical Chemistry of the Russian Academy of Sciences (GEOKhI RAS). A small-scale HD setup produced at the Bauman Moscow State Technical University by the group led by Professor V.N. Skorobogatskii [9] was used in the first experiments with chemically pure fluids of different molecular structures: benzene ( $\text{C}_6\text{H}_6$ ), toluene ( $\text{C}_6\text{H}_5\text{CH}_3$ ), and ethanol–aniline ( $\text{C}_2\text{H}_5\text{OH} + \text{C}_6\text{H}_5\text{NH}_2$  (3%)) mixtures. Nanodiamonds of various sizes were obtained in all cases: 20–30 nm (benzene), 10–15 nm (toluene), and 5–10 nm (ethanol–aniline) [10]. Benzene had the best carbon/hydrogen ratio, but it is a highly hazardous substance, and it proved problematic to work with it in a university setting. The presence of additional methyl groups alongside the aromatic ring was the advantage of toluene, since this provided more structural elements (seeds) for the diamond crystal lattice and, consequently, a higher yield of synthesized nanoparticles. The smallest nanodiamonds were obtained from the ethanol–aniline mixture. This indicated that diamond phase nuclei formed from molecular fragments rather than from atomic carbon vapor.

Unfortunately, the small HD setup created at the Bauman Moscow State Technical University had a number of significant shortcomings: experiments required a room certified for blasting, toxic and carcinogenic hydrocarbon fluids were used, and it was impossible to implement a continuous synthesis cycle. More detailed and accurate experiments combined with theoretical and numerical modeling were needed for further research into the mechanism of HD nucleation. Thus, a new modified setup for cavitation synthesis of nanodiamonds (UKNA), which utilizes the effect

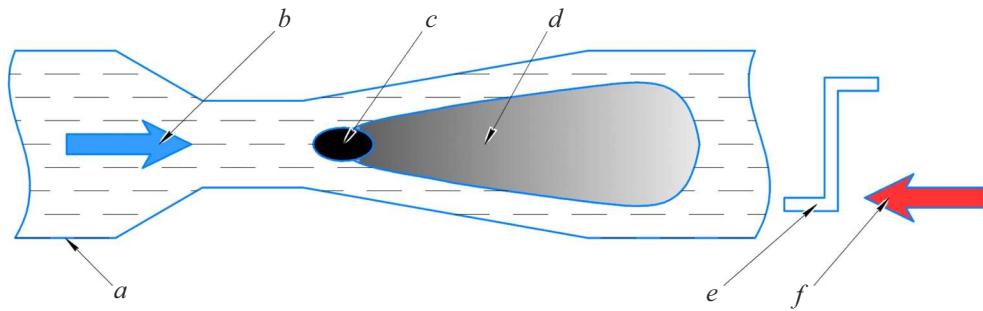


**Figure 1.** Scheme of operation of a nozzle that induces cavitation. *a* — Contoured nozzle, *b* — flow direction, *c* — insert, *d* — cavitation plume, *e* — pressure drop, and *f* — water hammer direction.

**Table 1.** Thermodynamic properties of working fluids

Working fluid	$P_{cr}$ , bar	$T_{cr}$ , K	$\rho_{cr}$ , kg/m <sup>3</sup>	$M$ , g/mol	$\gamma$	$\rho$ , kg/m <sup>3</sup>	$c$ , m/s
Water	221.2	374.12	317.8	18	1.325	998.2	1497 ( $c_2$ )
IPA	49	235	271	60	1.103	785	1247 ( $c_1$ )

Note.  $P_{cr}$ ,  $T_{cr}$ , and  $\rho_{cr}$  — physical quantities at the critical point: pressure, temperature, and density, respectively;  $M$  — molar mass;  $\gamma$  — adiabatic index; and  $\rho(c)$  — density (speed of sound) of the medium under normal conditions.

of a water hammer on cavitation bubbles in a circulating fluid flow, was constructed at GEOKhI RAS under the supervision of Academician E.M. Galimov. To accomplish this, the researchers had to establish a continuous cycle and provide a jump in external pressure sufficient for the adiabatic collapse of cavitation bubbles. The schematic diagram of the UKNA setup and a detailed description of its operation are presented in [11].

Its operating modes were analyzed using an HD model in ANSYS, where such process parameters as the transfer pump power, pipe diameters, flow velocity, and constriction dimensions were optimized, and a patent was obtained [12]. The key component of UKNA is a contoured nozzle with an adjustable insert that is used to form a stable cavitation plume. This plume is subjected to a water hammer (Fig. 1) produced by a high-speed shut-off valve with a pneumatic drive, which allows one to block completely the flow of a fluid moving at a velocity of  $\sim 6$  m/s in a fraction of a second. This provides a significant jump in external pressure (up to 15 bar), which was called a water hammer by Academician N.E. Zhukovsky [13].

Prior to experiments, we have simulated the compression of an individual bubble containing a mixture of water vapor and the vapor of one carbon-containing fluid: ethanol, acetonitrile, or isopropyl alcohol (IPA). The obtained results are detailed in [14]. These fluids were chosen for their fine solubility in water and low toxicity; their concentration, temperature, and the minimum water hammer magnitude required to produce a shock wave were varied in the calculations. The optimum conditions were established in modeling of a 3% IPA solution, where a shock wave in a bubble started to form already at a water hammer

magnitude of 10 bar. Therefore, this working mixture was the one chosen for further experiments. The calculated thermodynamic data for this solution are presented in Table 1.

The initial state of vapor in a bubble is determined by its radius and the composition of the mixture in which the concentration of the dissolved substance exceeds the concentration in the fluid due to greater volatility. For the gas mixture in a bubble, total pressure  $p_0$  at the initial moment is equal to the sum of pressures of vapor components. At the same time, according to Raoult's law, it is equal to the sum of pressures of saturated vapors with the corresponding weights:

$$p_0 = (v_1 + v_2)R_u T_0 / V_0$$

or

$$p_0 = v_1 p_{s1}(t_0) / (v_1 + v_2) + v_2 p_{s2}(t_0) / (v_1 + v_2), \quad (1)$$

where  $v_1$  and  $v_2$  are the numbers of moles of water vapor and IPA in a bubble,  $p_{s1}(t_0)$  and  $p_{s2}(t_0)$  are the saturated vapor pressure of water and the dissolved substance at temperature  $t_0$  (in °C),  $V_0$  is the initial bubble volume,  $T_0$  is the fluid temperature (in kelvin), and  $R_u$  is the universal gas constant.

Our calculations rely on a mathematical model in which the fluid is assumed to be weakly compressible and the vapor with a uniform distribution of thermodynamic parameters undergoes adiabatic compression by a water hammer with pressure jump  $-\Delta P$ . The variation of bubble radius  $R$  with time  $-R' = \partial R / \partial t$  is characterized by the

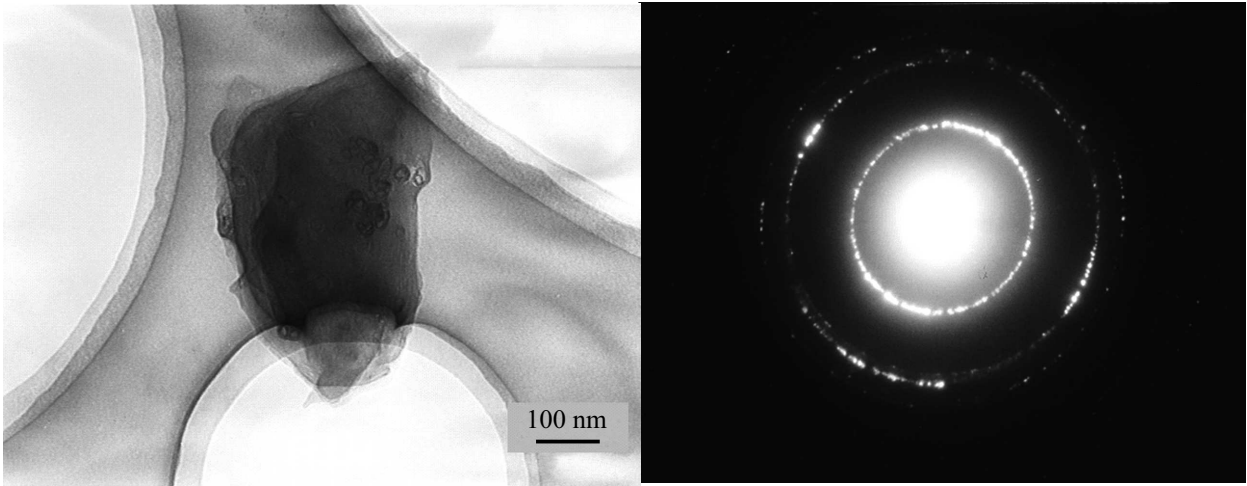


**Figure 2.** Image and electron diffraction pattern of a carbon particle (type 1).

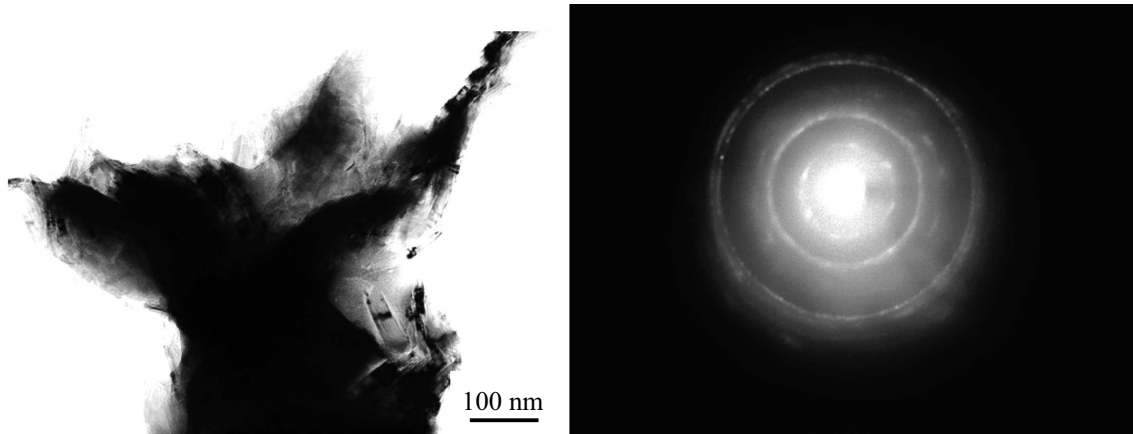


**Figure 3.** Image and electron diffraction pattern of a carbon particle (type 2).

Rayleigh–Plesset equation

$$(1 - R'/c)RR'' + 3/2(1 - R'/3c)(R')^2 = (1 - R'/c)(p - \Delta P)/\rho + R/c(p' - \Delta P')/\rho, \quad (2)$$

where  $p$  is the pressure of the gas mixture in a bubble,  $\rho$  is the density of the working fluid (water mixed with IPA), and  $c$  is the speed of sound in a solution with IPA concentration  $a$ ,

$$c = 1/[a/c_1 + (1 - a)/c_2]. \quad (3)$$

The pressure of the vapor mixture in a bubble is characterized by the modified van der Waals equation of state for each component with the use of data from Table 1.

Calculations are performed according to the procedure specified in [15], where the criterion of emergence of a shock wave in a bubble is the fulfillment of the following condition:

$$\min \Delta R_s / R < 1, \quad (4)$$

where  $\Delta R_s$  is the distance from the interphase boundary (bubble wall) to the point of origin of a shock wave in a bubble (the point of intersection of the characteristics characterizing the propagation of disturbance from the bubble surface). If  $\Delta R_s < R$ , a shock wave has enough time to form in a bubble during its collapse. In the contrary case, a shock wave does not form. The value of  $\Delta R_s$  is determined in the following way:

$$\Delta R_s = -(1 - R'/c_v)c_v^2/kR'', \quad k = 1 + \rho_v c'_v/c_v, \quad (5)$$

where  $\rho_v$  is the density of the gas mixture in a bubble near the wall, speed of sound  $c_v = \sqrt{\gamma_v p/\rho_v}$ , and  $c'_v$  is the partial derivative of the speed of sound with respect to density at constant entropy. Adiabatic index  $\gamma_v$  of the gas mixture in a bubble is given by

$$\gamma_v = 1 + (v_1 + v_2)/[v_1/(\gamma_1 - 1) + v_2/(\gamma_2 - 1)]. \quad (6)$$

Formulae (4) and (5) are valid in the planar problem; however, as was demonstrated in [15] by comparison with

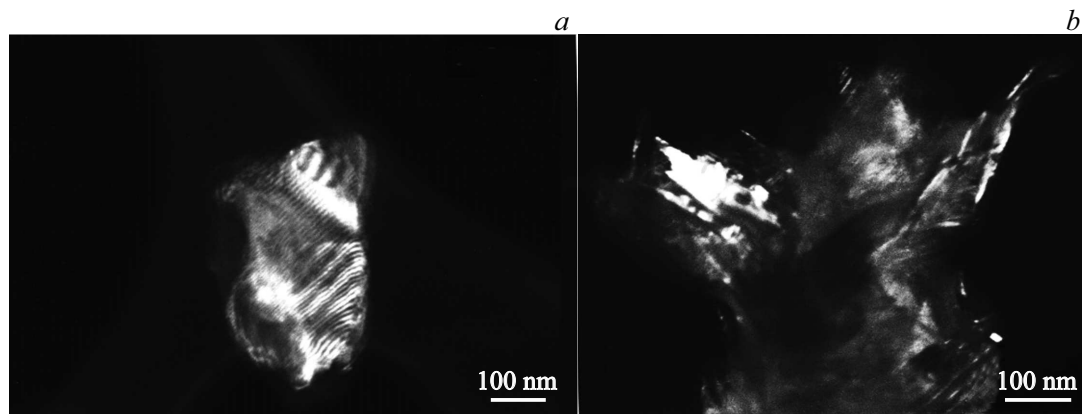


**Figure 4.** Dark-field images of carbon particles: in diamond (*a*) and graphite (*b*) reflections.

**Table 2.** Interplanar distances of NPs calculated by processing the electron diffraction patterns [16]

Reference				UKNA GEOKhI RAS			
indices indices (lattice of diamond, <i>Fd3m</i> )	Inter- planar dis- tance <i>d</i> , Å (lattice of diamond)	Miller indices, (lattice of graphite <i>P6<sub>3</sub>/mmc</i> )	Inter- planar dis- tance <i>d</i> , Å (lattice of graphite)	Cavitation carbon nanoparticles, $H_2O + C_3H_8O$			
				NPs type 1		NPs type 2	
				<i>d</i> , Å (experi- ment)	Phase	<i>d</i> , Å (experi- ment)	Phase
111	2.06	002	3.38	2.13	d	3.40	g
220	1.261	100	2.12	1.26	d	2.06	d
311	1.075	101	2.02	1.08	d	1.69	g
400	0.889	004	1.69			1.25	d
331	0.818	110	1.227	0.82	d	1.17	g
422	0.725	112	1.150	0.73	d		

Note: d — diamond, g — graphite.

the results of calculations based on the full hydrodynamic model, condition (4) is also applicable in the spherical case of a collapsing cavitation bubble.

Condition (4) ceases to be satisfied if the external pressure jump decreases or the fluid temperature increases. It should be noted that if a shock wave starts to form in a bubble, further calculations based on a zero-dimensional model (without full consideration of gas dynamics equations) are meaningless. The processes occurring during the collapse of a bubble in a mixture of water and IPA were calculated in accordance with [14] at a temperature of 20 °C and an external pressure of 10 and 15 bar, and the variation of parameter  $\Delta R_s/R$  in the process of compression of a bubble was determined as a function of its radius. It was demonstrated that the value of this parameter is minimized right before the compression stops, which occurs at the moment of maximum acceleration of the bubble wall toward compression (i.e., quantity  $-R''$ ). With a jump in external pressure  $\Delta P = 10$  bar, the system reaches boundary regime  $\Delta R_s/R \sim 1$ ; when the water hammer magnitude increases to  $\Delta P = 15$  bar, a shock wave propagates within

the bubble and nanodiamonds start to form instead of graphite nanoparticles.

To avoid a phase transition, the boundary regime with water hammer magnitude  $\Delta P = 10$  bar was used in synthesis of graphite composite stacks. Figures 2 and 3 show certain types of carbon nanoparticles (NPs) obtained in the experiment. All the obtained materials were examined with a JEM100CX11 transmission electron microscope by A.S. Aronin at the Institute of Solid State Physics of the Russian Academy of Sciences.

Figure 4 shows dark-field electron micrographs of cavitation NPs. Known data on the parameters of crystal lattices of graphite and diamond were used to analyze the structure of these NPs (Table 2).

The experimentally determined interplanar distance (111) for diamond particle type 1 is increased to 2.10–2.13 Å. The values of other interplanar distances agree well with the tabular ones (within the accuracy of the method). It is possible that impurities are embedded exactly between the (111) planes, since this distance exceeds the tabular values. Large bright regions and banded contrast are seen

in the dark-field images. The experimental data suggest the following possible explanation of structural features of NPs.

— Particles type 1 (nominally „diamond“ ones) consist of nanometer-thick layers with an in-plane size of hundreds of nanometers (bright regions in the dark-field image). The layers are stacked and rotated relative to each other. The banded contrast — moire contrast (phase contrast) — is indicative of layer rotation. The electron diffraction pattern of a particle of this type has distinct texture features: elongated and bifurcating rings. This fact is also indicative of a complex layered NP structure with the layers not being coordinated into a single crystal lattice; as a result, the reflections seen in the electron diffraction pattern are similar to those typical of a fine-grained object.

— Particles type 2 (nominally „graphene“ ones) have a fundamentally similar structure, but feature graphite layers in addition to diamond ones. Graphite layers (or graphite particles) produce an inner ring and three more rings in the electron diffraction pattern, as well as reflections in it (Figs. 3 and 4). Point reflections from graphite are also present.

Thus, the first experimental study of the effect of a water hammer of a boundary magnitude on a cavitating mixture of water and isopropyl alcohol was carried out. The formation of compounds and agglomerates of carbon nanoparticles with complex phase compositions (including composites containing graphene and diamond layers) was demonstrated qualitatively.

## Funding

This study was carried out under the state assignment of the Vernadsky Institute of Geochemistry and Analytical Chemistry of the Russian Academy of Sciences.

## Conflict of interest

The authors declare that they have no conflict of interest.

## References

- [1] A.K. Geim, A.H. MacDonald, *Phys. Today*, **60**, 35 (2007). DOI: 10.1063/1.2774096
- [2] L.A. Ponomarenko, F. Schedin, M.I. Katsnelson, R. Yang, E.W. Hill, K.S. Novoselov, A.K. Geim, *Science*, **320** (5874), 356 (2008). DOI: 10.1126/science.1154663
- [3] A.K. Geim, K.S. Novoselov, *Nat. Mater.*, **6**, 183 (2007). DOI: 10.1038/nmat1849
- [4] S. Gilje, S. Han, M. Wang, K.L. Kang, R.B. Kaner, *Nano Lett.*, **7**, 3394 (2007). DOI: 10.1021/nl0717715
- [5] A. Kunznetsova, I. Popova, J. Yates, M.J. Bronikowski, C.B. Huffman, J. Liu, R.E. Smalley, H.H. Hwu, J.J. Chen, *J. Am. Chem. Soc.*, **123**, 10699 (2001). DOI: 10.1021/ja011021b
- [6] D. Li, M.B. Muller, S. Gilje, R.B. Kaner, G.G. Wallace, *Nat. Nanotechnol.*, **3**, 101 (2008). DOI: 10.1038/nnano.2007.451
- [7] S.A. Voropaev, N.V. Dushenko, A.Yu. Dnestrovskiy, A.P. Krivenko, *Geochem. Int.*, **59** (11), 1052 (2021). DOI: 10.1134/S0016702921110112.
- [8] E.M. Galimov, *Nature*, **243**, 389 (1973). DOI: 10.1038/243389a0
- [9] É.M. Galimov, A.M. Kudin, V.N. Skorobogatskii, V.G. Plotnichenko, O.L. Bondarev, B.G. Zarubin, V.V. Strazdovskii, A.S. Aronin, A.V. Fisenko, I.V. Bykov, A.Yu. Barinov, *Dokl. Phys.*, **49**, 150 (2004). DOI: 10.1134/1.1710678.
- [10] S.A. Voropaev, A.Yu. Dnestrovskii, V.N. Skorobogatskii, A.S. Aronin, V.M. Shkinev, O.L. Bondarev, V.V. Strazdovskii, A.A. Eliseev, E.A. Zevakin, E.A. Ponomareva, E.M. Galimov, *Dokl. Phys.*, **56** (9), 463 (2011). DOI: 10.1134/S1028335811090126.
- [11] N.V. Dushenko, S.A. Voropaev, E.A. Ponomareva, A.Yu. Dnestrovskii, V.M. Shkinev, A.S. Aronin, E.M. Galimov, *Izv. Vyssh. Uchebn. Zaved., Khim. Khim. Tekhnol.*, **59** (9), 80 (2016).
- [12] S.A. Voropaev, N.V. Dushenko, *Sposob polucheniya ul'tradispersnykhalmazov i ustanovka dlya ego osushchestvleniya*, RF Patent No. 2784236C1 (applied on September 28, 2021; published on November 23, 2022) (in Russian).
- [13] N.E. Zhukovskii, *O gidravlicheskom udare v vodoprovodnykh trubakh* (Izd. Mosk. Univ., M., 1898) (in Russian).
- [14] A.Yu. Dnestrovskij, S.A. Voropaev, N.V. Dushenko, S.G. Naimushin, E.M. Galimov, *Dokl. Phys.*, **65** (1), 8 (2020). DOI: 10.1134/S1028335820010097.
- [15] R.I. Nigmatulin, A.A. Aganin, D.Yu. Toporkov, M.A. Il'gamov, *Dokl. Phys.*, **59** (9), 431 (2014). DOI: 10.1134/S1028335814090109.
- [16] B.K. Vainshtein, A.A. Chernov, L.A. Shuvalov, *Sovremennaya kristallografiya. Struktura kristallov* (Nauka, M., 1979) (in Russian).

Translated by D.Safin